Structure, Vol. 13, 1385–1396, September, 2005, ©2005 Elsevier Ltd All rights reserved. DOI 10.1016/j.str.2005.05.016

The Structure of a Eukaryotic Nicotinic Acid Phosphoribosyltransferase Reveals Structural Heterogeneity among Type II PRTases

Joshua S. Chappie,[1,2,5] Jaume M. Cànaves,[1,3,5] Gye Won Han,[1,2] Christopher L. Rife,[1,4] Qingping Xu,[1,4] and Raymond C. Stevens[1,2,*]
[1]The Joint Center for Structural Genomics
[2]The Scripps Research Institute
10550 North Torrey Pines Road
La Jolla, California 92037
[3]University of California, San Diego
9500 Gilman Drive
La Jolla, CA 92093
[4]Stanford Synchrotron Radiation Laboratory
Stanford University
2575 Sand Hill Road
SSRL MS 99
Menlo Park, California 94025

Summary

Nicotinamide adenine dinucleotide (NAD) is an essential cofactor for cellular redox reactions and can act as an important substrate in numerous biological processes. As a result, nature has evolved multiple biosynthetic pathways to meet this high chemical demand. In *Saccharomyces cerevisiae*, the NAD salvage pathway relies on the activity of nicotinic acid phosphoribosyltransferase (NAPRTase), a member of the phosphoribosyltransferase (PRTase) superfamily. Here, we report the structure of a eukaryotic (yeast) NAPRTase at 1.75 Å resolution (locus name: YOR209C, gene name: NPT1). The structure reveals a two-domain fold that resembles the architecture of quinolinic acid phosphoribosyltransferases (QAPRTases), but with completely different dispositions that provide evidence for structural heterogeneity among the Type II PRTases. The identification of a third domain in NAPRTases provides a structural basis and possible mechanism for the functional modulation of this family of enzymes by ATP.

Introduction

Nicotinamide adenine dinucleotide (NAD) is a versatile compound that participates in a host of biological functions. Acting as an electron shuttle, it serves as an essential cofactor for cellular redox reactions and energy metabolism (Rizzi and Schindelin, 2002). Additionally, NAD can be utilized as a consumable substrate to modulate other significant biological activities, including transcriptional regulation, DNA damage response, and neuroprotection (Pappas et al., 2004; Buck et al., 2004; Muiras, 2003; Araki et al., 2004). Enzymes that employ NAD in this fashion include the Sir2 family of protein deacetylases (Sirtuins) and poly(ADP-ribose) polymerases (PARPs). To sustain these demanding chemical roles, organisms must maintain a constant reservoir of NAD. In most cases, including in humans and in yeast, NAD replenishment is primarily achieved through de novo biosynthesis (Figure 1, black). The initial step of this pathway is catalyzed by quinolinic acid phosphoribosyltransferase (QAPRTase), which forms the NAD precursor nicotinic acid mononucleotide (NAMN) from the tryptophan metabolite quinolinic acid (QA). Alternatively, NAD can be synthesized from NA via the Preiss-Handler pathway (Preiss and Handler, 1958a, 1958b) (Figure 1, dashed blue). This series of reactions helps facilitate the dietary uptake of NA by converting it to the usable substrate NAMN, the point of convergence with the de novo pathway. Salvage pathways, which recover NAD from its degradation product nicotinamide (NM), also exist (Katoh and Hashimoto, 2004). Organisms that contain nicotinamide deaminase, such as yeast and *E. coli*, are able to convert NM back to NA and exploit the Preiss-Handler pathway for salvage purposes (Figure 1, solid blue). Vertebrates, however, lack this enzyme, and their NAD salvage functions are dependent on the activity of nicotinamide phosphoribosyltransferase (NMPRTase). This salvage route recycles NAD through the intermediate nicotinamide mononucleotide (NMN) (Figure 1, red). Other bacteria, such as *Haemophilus influenza*, lack the enzymes of the aforementioned pathways and, instead, use an alternate biosynthetic mechanism involving ribosyl nicotinamide (RN) and NMN, a process shown to be present in eukaryotes as well (Bieganowski and Brenner, 2004) (Figure 1, green).

In the yeast *Saccharomyces cerevisiae*, the NAD salvage pathway relies on the activity of NAPRTase. As a member of the phosphoribosyltransferase (PRTase) superfamily, this enzyme employs 5′-phosphoribosyl-1′-pyrophosphate (PRPP) as a substrate to catalyze the first reaction in the Preiss-Handler pathway:

$$NA + PRPP \rightleftharpoons NAMN + PP_i$$

The rate of this reaction is quite slow at 0.3 s^{-1}, rendering this enzyme thoroughly inefficient on its own. To circumvent this problem, NAPRTases couple ATP hydrolysis to their transferase activity, thereby increasing the catalytic turnover to 500 s^{-1} (Gross et al., 1998; Grubmeyer et al., 1999). This stimulation occurs through the phosphorylation of a specific, conserved histidine residue in a process that thus far appears to be unique to the NAPRTase family. Mutational studies indicate that changing this residue completely abrogates both autophosphorylation and ATP-dependent stimulation (Gross et al., 1996; Rajavel et al., 1998). This implies that NAPRTases are subject to three competing reactions at any one time: basal catalysis, stimulated catalysis, and ATP hydrolysis.

In spite of this well-understood kinetic scheme, a detailed description of NAPRTase structure has remained elusive. A number of other PRTases have been determined at high resolution and have revealed distinct structural classes based on overall fold and conserved

*Correspondence: stevens@scripps.edu
[5]These authors contributed equally to this work.

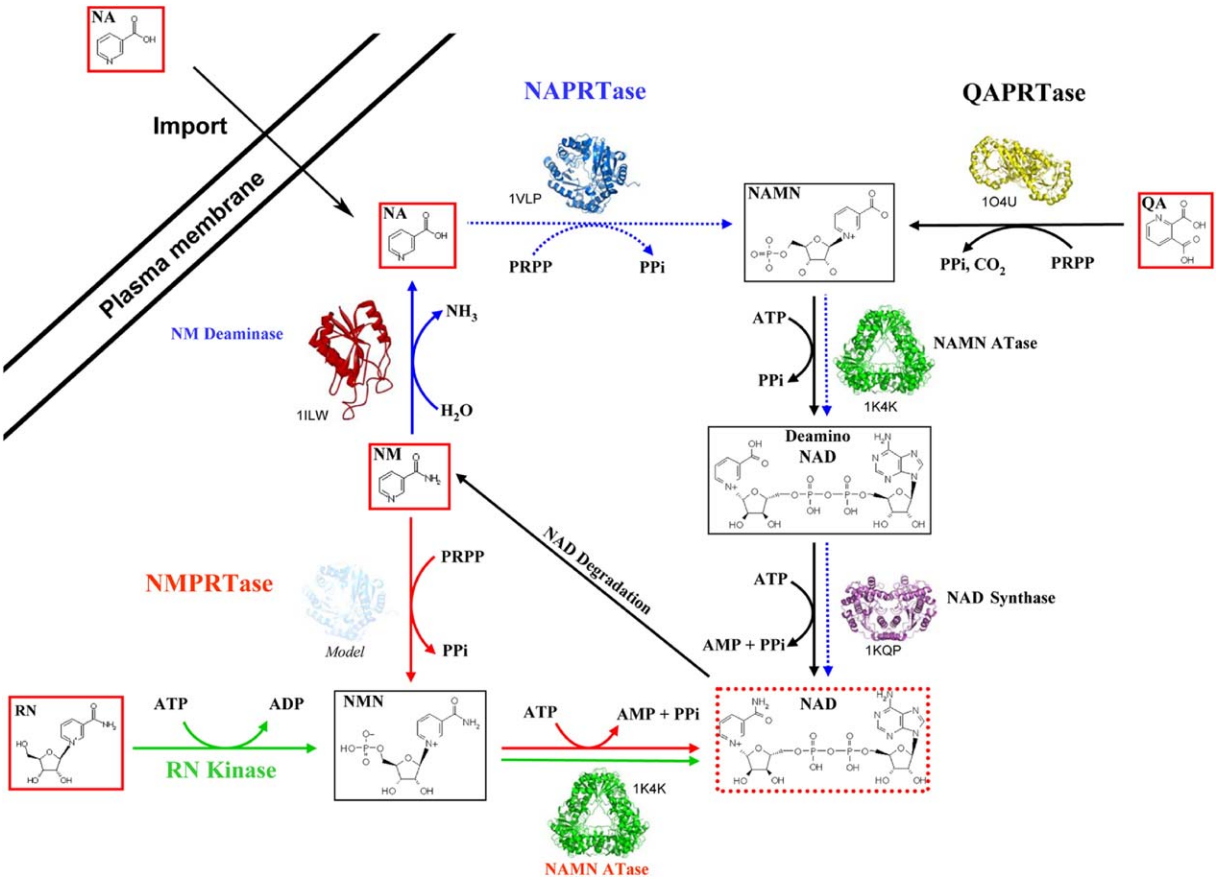

Figure 1. NAD Biosynthetic Pathways

Solid black arrows indicate the de novo biosynthesis pathway, dashed blue arrows indicate the Preiss-Handler pathway, the solid blue arrow indicates the salvage route using nicotinamide deaminase, solid red arrows indicate the NMPRTase-dependent salvage pathway, and solid green arrows indicate the nicotinamide riboside pathway. For each step in the reaction scheme, PDB codes and structures are provided (where applicable). Boxed molecules represent major metabolic substrates/products. Abbreviations are as follows: QA, quinolinic acid; NA, nicotinic acid; NAMN, nicotinic acid mononucleotide; NAD, nicotinamide adenine dinucleotide; NM, nicotinamide; NMN, nicotinamide mononucleotide; RN, ribosyl nicotinamide; PRPP, 5′-phosphoribosyl-1′-pyrophosphate; PRTase, phosphoribosyltransferase; ATase, adenylyltransferase.

characteristics. Type I PRTases contain a five-stranded, parallel β sheet surrounded by α helices (the "PRTase fold") and a common PRPP binding motif (Vos et al., 1997). Type II PRTases, represented in the Protein Data Bank (PDB) by several bacterial QAPRTases, exhibit an irregular seven-stranded α/β barrel and an N-terminal open-faced sandwich. Members of this group lack the conserved PRPP binding site and instead have a phosphate binding motif that resembles that of unrelated enzymes (Eads et al., 1997; Sharma et al., 1998; Schwarzenbacher et al., 2004). Other structural examples outside the Type I/Type II PRTase framework include the anthranilate PRTase, with a two-domain fold that encompasses a seven-stranded mixed β sheet (Mayans et al., 2002; Kim et al., 2002), and the ATP PRTase, comprised of three continuous domains that each contain a β sheet surrounded by α helices (Cho et al., 2003). From sparse sequence conservation, it has been suggested that NAPRTase architecture is akin to that of the QAPRTases, which would classify it as a Type II PRTase (Rajavel et al., 1998). More recently, the structure of the *Thermoplasma acidophilum* NAPRTase was also reported (Shin et al., 2005).

In this work, we have used X-ray crystallography to determine the structure of the NAPRTase from *Saccharomyces cerevisiae* (yNAPRTase) at 1.75 Å resolution. To our knowledge, this structure represents the first high-resolution view of a eukaryotic Type II enzyme and the second published example of an NAPRTase structure (Shin et al., 2005). The two-domain fold of yNAPRTase confirms a general similarity to QAPRTases; however, the barrel and sandwich domains occupy different relative dispositions to one another, permitting the NAPRTase to exist in an alternative oligomeric state. We have further analyzed residue, domain, and site conservation among Type II PRTases, as well as phylogenetic and structural relationships within this enzyme family. These combined data suggest a possible molec-

Table 1. Summary of Crystal Parameters, Data Collection, and Refinement Statistics for yNAPRTase

	λ_0Se	λ_1MADSe	λ_2MADSe
Data Collection			
Space group	P_1	P_1	P_1
Unit cell parameters	a = 54.406 Å, b = 83.103 Å, c = 107.237 Å, α = 97.35°, β = 95.67°, γ = 97.99°	a = 54.706 Å, b = 83.143 Å, c = 107.502 Å, α = 97.29°, β = 95.01°, γ = 97.88°	a = 54.406 Å, b = 83.103 Å, c = 107.237 Å, α = 97.35°, β = 95.67°, γ = 97.99°
Wavelength (Å)	0.96860	0.97980	1.0332
Resolution range (Å)	50.00–1.75	50.00–2.02	50.00–2.13
Number of observations (>1)	667,108	439,886	383,937
Number of reflections	177,740	118,673	101,313
Completeness (%)	96.8	97.5	97.5
Mean I/σ(I)	10.1	8.1	9.9
R_{sym} on I	0.075	0.118	0.104
Sigma cutoff	0.0	0.0	0.0
Highest-resolution shell (Å)	1.81–1.75	2.09–2.02	2.21–2.13
Model and Refinement Statistics			
Data set used in refinement	λ_0Se		
Cutoff criteria	|F| > 0		
R_{cryst}	0.1696		
R_{free}	0.2096		
Resolution range (Å)	48.22–1.75		
Number of reflections (total)	168,817		
Number of reflections (test)	8,921		
Completeness (% total)	96.2		
Stereochemical Parameters			
Restraints (rms observed)			
Bond length	0.018 Å		
Bond angle	1.54°		
Average isotropic B value	8.5 Å^2		
ESU based on R value	0.112 Å		
Protein residues/atoms	1671/13,455		
Solvent molecules	1,272		

Atomic coordinates and experimental structure factors of yNAPRTase have been deposited with the PDB and are accessible under the code 1VLP. High resolution data set (λ_0Se) and MAD data sets (λ_1MADSe and λ_2MADSe) were collected on two separate crystals. ESU = estimated overall coordinate error (CCP4, 1994; Tickle et al., 1998). $R_{sym} = \Sigma|I_i - \langle I_i\rangle|/\Sigma|I_i|$, where I_i is the scaled intensity of the i^{th} measurement, and $\langle I_i\rangle$ is the mean intensity for that reflection. $R_{cryst} = \Sigma||F_{obs}| - |F_{calc}||/\Sigma|F_{obs}|$, where F_{calc} and F_{obs} are the calculated and observed structure factor amplitudes, respectively. R_{free} = as for R_{cryst}, but for 5.0% of the total reflections chosen at random and omitted from refinement.

ular evolution mechanism that can contribute to our understanding of the evolution of NAD biosynthetic and salvage pathways.

Results and Discussion

Structure of NAPRTase

Native yNAPRTase is a 430 residue protein with a calculated molecular mass of 49 kDa. The final model contains four protein monomers in the asymmetric unit (designated as molecules A, B, C, and D), each containing residues 1–415 (B and C extend to 419 and 416, respectively). The four individual monomers are structurally equivalent and superimpose with an average rmsd of 0.33 Å when aligned with the multiple structural alignment program MASS (Dror et al., 2003). The Matthews' coefficient, V_m (Matthews, 1968), for yNAPRTase is 2.29 Å^3/Da, and the estimated solvent content is 45.8%. According to the Ramachandran plot, 91.2% of the residues fall within the most favored regions, while the remaining 8.8% occupy additionally allowed regions. A summary of the crystal parameters, data collection, and refinement statistics are outlined in Table 1 (see Experimental Procedures).

The overall architecture of each yNAPRTase monomer consists of 13 β strands, 19 α helices, and two 3_{10} helical segments (H3 and H15) (Figures S1A and S1B; see the Supplemental Data available with this article online). These elements are organized into two domains: a discontinuous open-faced α + β sandwich, and an irregular α/β barrel (Figure 2A). The β sandwich domain is composed of the N-terminal residues 2–148 and an additional segment that flanks the barrel domain on the C-terminal edge (residues 360–383). The upper portion of the fold is an antiparallel β sheet (strands β1, β2, β3, β12), which rests atop a helical assembly (H1–8) that closes the barrel. This sandwich arrangement is a common feature among glycosyltransferases. Domain B (residues 149–359, shown in cyan in Figure 2A), in contrast, has a barrel design that is shared only with members of the QAPRTase family. Eight helices (H9, H10, H12–H14, H16, H18, and H19) line the perimeter of the barrel core, which is composed of strands β4–β9. A gap exists between the second and third strands, causing an irregular distribution of the barrel components around the central axis. An additional structural element, domain C (shown in magenta in Figure 2A), extends from the final β strand of the sandwich region

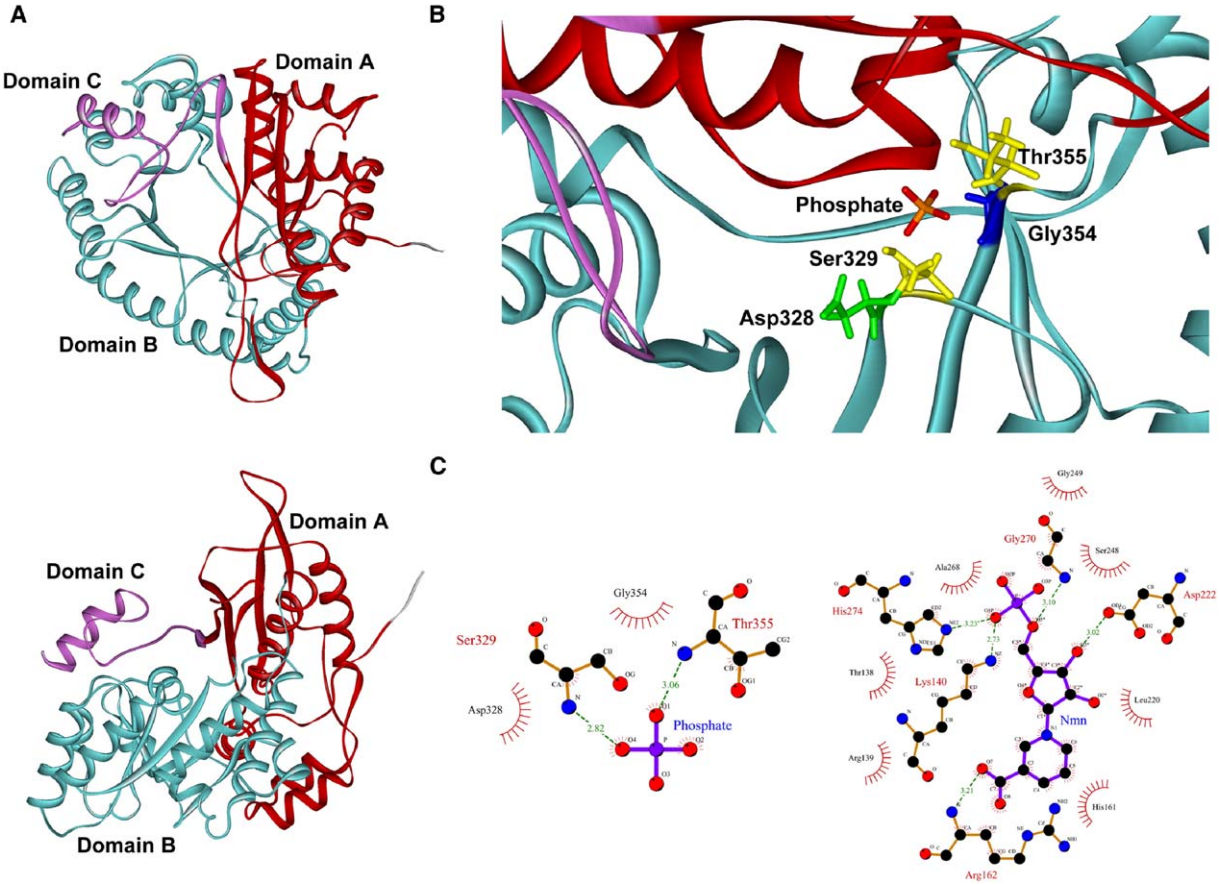

Figure 2. Structure and Active Site of yNAPRTase

(A) Top and side views of the yNAPRTase monomer. Domains A, B, and C are colored red, cyan, and magenta, respectively.

(B) Magnified view of a bound phosphate molecule. The phosphate molecule is colored in red. Side chains participating in hydrogen bonding (S329 and T355) are depicted in yellow, while those involved in van der Waals interactions (D328 and G354) are shown in green and blue. Three-dimensional rendering generated with Accelrys Discovery Studio ViewerPro 5.0.

(C) Comparison of bound phosphate in yNAPRTase (left) with the *M. tuberculosis* QAPRTase active site (right; nicotinate mononucleotide substrate). The binding interactions are shown in two dimensions via Ligplot; dashed lines represent hydrogen bonds, and semi-circles with straight lines denote van der Waals interactions.

and constitutes a novel feature thus far only observed in NAPRTases. This C-terminal appendage (residues 383–415) contains a short β strand (β13), a long unstructured coiled region, and an α helix. Markedly absent in this arrangement are the "PRTase fold" and the conserved binding motif common to Type I PRTases. Since the classification of PRTases reflects shared structural features, the observed structural similarity to QAPRTases, the archetypal Type II enzymes, implicates yNAPRTase as another unique example of a Type II PRTase.

Active Site Conservation

In the yNAPRTase crystal, a single phosphate molecule is bound to each protein monomer. The ligand is positioned above β9 in the barrel domain and hydrogen bonds with the backbone amides of S329 and T355. Additional van der Waals contacts are made by D328 and G354 (Figures 2B and 2C, left). Sequence alignment shows that three of these side chains (D328, G354, and T355) are absolutely conserved across the entire NAPRTase family. Since phosphate alone is not a functional substrate of the NAPRTase enzyme, it is difficult to define unambiguously the active site of yNAPRTase. However, the positioning of this molecule in the barrel domain helps to establish a contextual framework for the catalytic center via comparison with other Type II PRTases. Figure 2C (right) illustrates the key binding interactions in the *Mycobacterium tuberculosis* QAPRTase (PDB: 1QPR) (Sharma et al., 1998). This structure contains bound PRPP and QA analogs, which are situated across the top of the barrel core and are coordinated by loop residues, waters, and metal ions. When this assembly is juxtaposed with comparable regions in yNAPRTase, the 5′-phosphate of PRPP coincides with the location of the free phosphate, thereby defining the lower edge of the NAPRTase active site. This same position is occupied by a lone sulfate ion in the apo structure of the *M. tuberculosis* QAPRTase (PDB: 1QPO) (Figure S4). Through this structural align-

ment, one might expect that the unoccupied area near the upper perimeter of the yNAPRTase barrel would contain the NA binding site. In the yNAPRTase crystal, this region (between β12 and H13) contains a solvent-filled cavity occupied by several ordered water molecules (Figures S4A and S4B). Comparison to the *M. tuberculosis* apo structure reveals a similar cavity that is also solvent exposed (occupied by three waters) (Figure S4C). Upon binding, the QA analog supplants two of these molecules, which fill the void in its absence (Figure S4D). It can therefore be assumed that the binding of NA would have a similar result, given the similarity of the substrates and domain conservation between these two enzyme families. The common arrangement of these binding sites is further reflected in the surrounding side chains. A sequence output from a flexible structural alignment of the yeast NAPRTase and the *M. tuberculosis* QAPRTase reveals that residues participating in QA and NAMN binding in QAPRTases superimpose with chemically related side chains in the NAPRTase structure. Of 16 residues implicated in QA or NAMN binding in the *M. tuberculosis* QAPRTase, 3 are fully conserved, but another 8 show some degree of conservation based on their physicochemical properties (Figure S5). Together, these results show that the active sites of QAPRTases and NAPRTases are structurally related despite differences in relative domain orientation and very low sequence similarity.

Predicted ATP Binding Site

Intensive functional examination of the NAPRTase family has revealed that ATP increases the efficiency of catalysis through autophosphorylation of a conserved histidine residue (H232 in yNAPRTase) (Gross et al., 1996, 1998; Rajavel et al., 1998). Attempts to visualize the ATP binding site by cocrystallization with either ATP or the nonhydrolyzable ATP analog AMPPNP (adenosine 5′-(β,γ-imido)triphosphate) yielded only tiny microcrystals. Seeding these complexes increased the crystal size, but failed to improve diffraction quality, as was also the outcome for soaking experiments. To determine the possible location of the ATP binding pocket in the yNAPRTase structure, a novel tool called SiteEngine was employed (Shulman-Peleg et al., 2004). For this analysis, the ATP binding motif of the *M. tuberculosis* ATP PRTase (PDB: 1NH8) was selected, as this protein binds both ATP and PRPP. The best solution for ATP binding in the yNAPRTase structure corresponds to a loop region (residues I389, K390, N394, L395, K397, G400, and D401) located in domain C. Such an approximation would place H232 in direct contact with the α phosphate, while the β and γ phosphates would interact with residues L269 and D296, respectively (Figure 3A). A survey of 29 NAPRTase sequences shows that the position homologous to D296 is 100% conserved, and that the homologous position to L269 is conserved in all sequences, except in the NAPRTase from *Vibrio cholerae*, where a proline is present (a leucine located four positions toward the carboxy terminus could play the role of L269 in that protein). The proposed location of this binding site is consistent with previous studies showing that domain C is solvent accessible and capable of undergoing an ATP-dependent conformational change that protects against proteolytic cleavage (Rajavel et al., 1996). In yNAPRTase, the loop region of domain C exists in two conformations, supporting the notion of its inherent flexibility (Figure 3B). One might envision that this loop can reorient itself into a locked conformation upon ATP binding so as to create a local environment that favors autophosphorylation at H232.

Addition of this ATP binding pocket is a key evolutionary difference that distinguishes NAPRTases from QAPRTases. A structural alignment between yNAPRTase with the *Salmonella typhimurium* QAPRTase (PDB: 1QAP) using the Combinatorial Extension of optimal path (CE) method (Shindyalov and Bourne, 1998) reveals that H232 in yNAPRTase is analogous to E214 in the QAPRTase. Multiple sequence alignment of 20 QAPRTases from bacteria, archaea, and eukarya shows that this glutamic acid is strictly conserved (data not shown). By comparison with the proposed catalytic mechanisms of orotate PRTase and hypoxanthine-guanine PRTase, E214 is possibly involved in stabilization of a positively charged transition state in QAPRTases (Eads et al., 1994). In NAPRTases, the electrostatic stabilization of a positively charged intermediate via the same mechanism would only be possible after the addition of a negative charge to H232 through autophosphorylation. This improved transition state stabilization could easily translate into the ATP-dependent catalytic stimulation observed for NAPRTases, a phenomenon absent in QAPRTases (Hughes et al., 1993; Cao et al., 2002). The localization of the ATP binding site to domain C would rationalize these findings, as QAPRTases lack this structural element. Since tight energetic coupling espouses effective catalysis in NAPRTases, the additional regulation bestowed by domain C may further stipulate the functional context of these enzymes within NAD biosynthetic pathways.

Comparison of Oligomeric States

With the high degree of sequence homology among the sandwich and barrel domains of Type II PRTases, one would also expect their tertiary and quaternary interactions to be similar. However, structural comparison of these two enzyme families reveals distinct differences in three-dimensional organization. A structural alignment of the yNAPRTase monomer with the *S. typhimurium* QAPRTase was carried out with the CE method (Shindyalov and Bourne, 1998). This structural alignment, which treats each monomer as a rigid body, shows a tight superimposition of the barrel domains in each structure (Figure 4A). The sandwich domains, in contrast, occupy extremely different dispositions that cap the barrel in the yNAPRTase structure while protruding outward in QAPRTases. The alternative positioning of these segments in each enzyme facilitates the formation of different oligomers: yNAPRTase exists as a closed monomer, whereas all known QAPRTase structures form head-to-tail, domain-swapped dimers (Figures 1A and 4B; Schlunegger et al., 1997). It is feasible that this molecular pairing in QAPRTases is driven by the formation of an open monomer coupled with the motivation to maintain the integrity of interface contacts between the barrel and sandwich domains (Figure 4B).

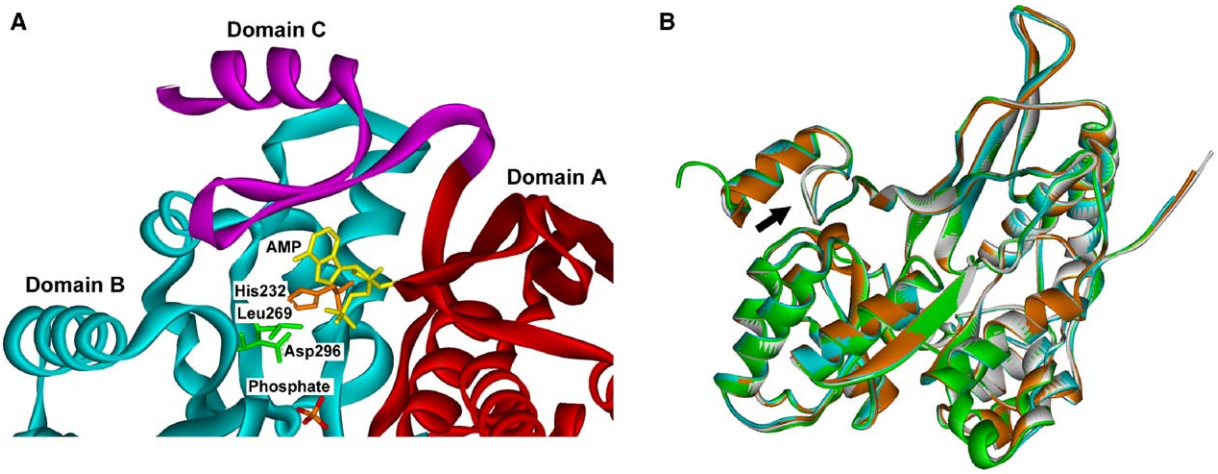

Figure 3. ATP Binding in yNAPRTase

(A) View of the predicted ATP binding site from a SiteEngine search. Loop residues of domain C (shown in magenta) help position the adenosine ring, allowing the phosphates to extend into the barrel cavity to interact with the autophosphorylatable H232 (orange), as well as L269 and D296 (green). AMP is modeled into the binding pocket. The bound phosphate ligand (presumably indicating the PRPP binding site) is shown. Domains are colored as in Figure 1.

(B) Superposition of the four molecules of yNAPRTase in the asymmetric unit (colored cyan, orange, green, and white) reveals the inherent flexibility of the domain C loop. This segment occupies two distinct conformations in the crystal (signified by a black arrow), one of which is present in molecules A and B, the other being found in molecules C and D.

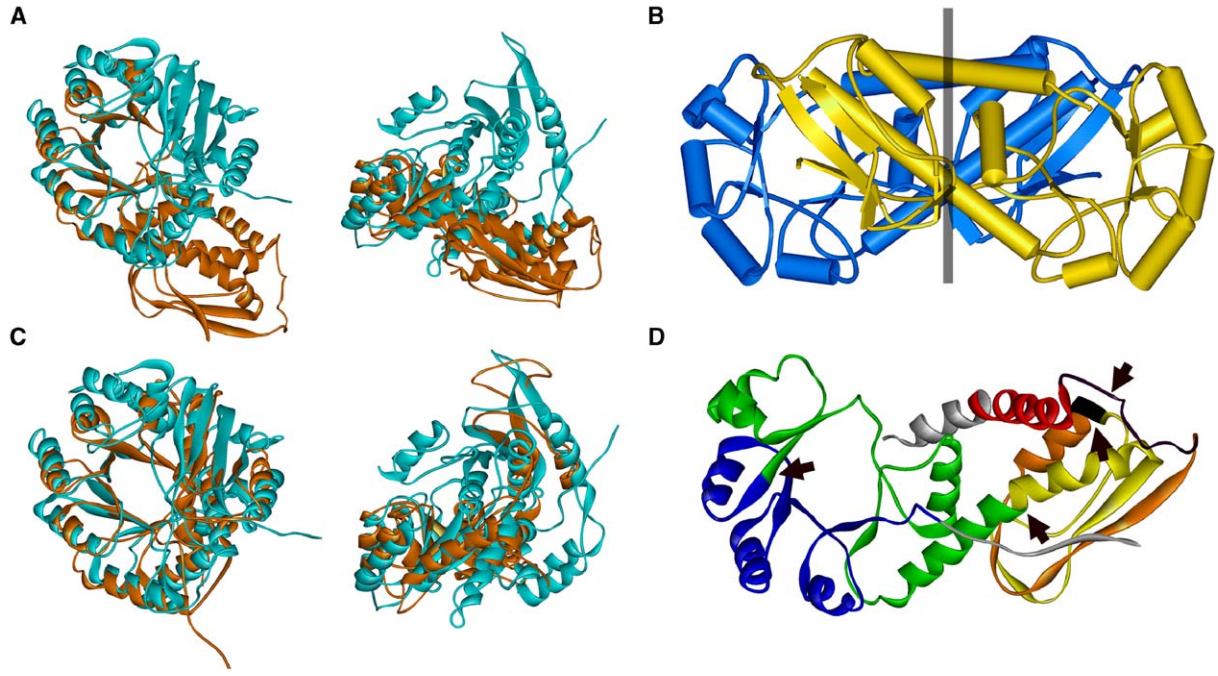

Figure 4. Rigid and Flexible Alignments of yNAPRTase and *S. typhimurium* QAPRTase Monomers

(A) Rigid structural alignment using the CE method. The yNAPRTase monomer (PDB: 1VLP) is colored cyan, the *S. typhimurium* monomer (PDB: 1QAP) is colored orange.

(B) Head-to-tail dimeric arrangement common to QAPRTases. The *S. typhimurium* dimer is shown with monomers colored blue and yellow to differentiate. The black line indicates the preservation of interdomain contacts found in the yNAPRTase monomer through domain swapping (compare to Figure 1A).

(C) Flexible structural alignment of monomers by using FATCAT. Monomers are colored as in (A).

(D) Location of the four twists (denoted as black arrows) introduced into the QAPRTase monomer that facilitate agreement of the two structures by flexible alignment.

Table 2. FFAS03 Search Results for NMPRT

Enzyme	PDB Code	Score	Identity
Saccharomyces cerevisiae NAPRTase	1VLP	–65.0	14%
Helicobacter pylori QAPRTase	1S41	–28.5	10%
Salmonella typhimurium QAPRTase	1QAP	–24.9	13%
Mycobacterium tuberculosis QAPRTase	1QPN	–24.1	16%
Thermotoga maritima QAPRTase	1O4U	–19.9	10%

The FFAS03 search was performed by using the sequence of mouse NMPRTase as query. A score of –9.5 is the significance threshold for this tool, indicating that less than 3% of the matches are false positives. The more negative the score, the better the match.

FATCAT (Ye and Godzik, 2003), an alternative structural alignment method that permits mobility in and between structural components, reveals a common architectural blueprint that transcends domain organizational differences (Figures 4C and 4D). This flexible approach significantly improves the alignment of the two structures by introducing four twists in the QAPRTase structure. The twist points used for manipulation (arrows), which are depicted in a rainbow scheme in Figure 4D, occur between five conserved regions in the QAPRTase structure. The first twist, shown in black, is located in a nonconserved linker between the red and orange segments. The second twist, also colored black, contains nonconserved residues linking the orange and yellow sections of the sandwich domain. The final two twists occur at the bend of the long α helix that connects the two domains and within the barrel structure in β7. The result is a robust matching of the key structural elements between the two enzymes, with only minor gaps in the alignment.

In NAPRTases, domains A and B are permanently in close contact, and the enzymatic activity is modulated by domain C-dependent autophosphorylation. In QAPRTases, where this regulation is absent, it is tempting to speculate that the control of the enzymatic activity might be accomplished through a monomer (inactive)-to-dimer (active) transition driven by the interaction between the A and B domains. Such transitions in oligomeric state have been observed in other PRTases, such as uracil PRTase (Jensen et al., 1997) and anthranilate 5-PRPP PRTase (Marcus and Balbinder, 1972).

Implications for Other NAD Salvage Enzymes

The architectural distinctions highlighted by the yNAPRTase structure raise an important question: how well do these features extend to other salvage enzymes involved in NAD recycling? As illustrated in Figure 1, an additional recycling route produces NAD from NM in a two-step mechanism mediated by NMPRTases. Little is known about the structure and function of this enzyme family, although it has been linked to lymphocyte activation and transcriptional regulation via Sir2 proteins (Rongvaux et al., 2002; Revollo et al., 2004). To determine whether NMPRTases have any structural homology to the other NAD biosynthetic PRTases, a BLAST search with the mouse NMPRTase sequence (GenBank: GI:10946948) against the PDB database was performed. No significant matches were obtained (the best expectation value was 1.2). Therefore, we resorted to using the Fold and Function Assignment System (FFAS03), a sensitive profile-profile fold recognition method (Rychlewski et al., 2000), to search the mouse NMPRTase sequence against the PDB database. This technique, which utilizes entire homologous families to create protein profiles for a matching algorithm, is able to detect distant homologies that are often missed due to low sequence identity. The results for this search are illustrated in Table 2, with a more negative score signifying a better statistical match between a query sequence and a characterized fold. The typical significance threshold is –9.5, which indicates that less than 3% of the matches are false positives. Of all possible protein folds, the best match for the NMPRTase is the yNAPRTase monomer, with a score of –65.00 (14% sequence identity). More distant fold matches also occur with the four known QAPRTase structures (Table 2), which can be expected due to the common structural domains among Type II PRTases. The implication of this finding is that NMPRTases can be classified as Type II PRTases and suggests that they are more likely to adopt the closed monomer configuration of NAPRTases, with whom they are more closely related. Based on this hypothesis, the yNAPRTase structure was employed as a template to generate a homology structural model for the NMPRTase (Figure 5A) by using the program Modeller (Fiser and Sali, 2003) and the FFAS03 alignment (Figure S2A).

The homology model of the mouse NMPRTase provides two key insights into the structural properties of Type II PRTases. First, it helps further define a conserved tripartite sequence motif that forms the interface between domains A and B (Figure S2B). This consensus site is reasonably well conserved between all three families, with diverging residues showing a greater degree of similarity within each individual enzyme type. These contacts are maintained independently of the oligomeric state. It is feasible that given the irregular arrangement of the barrel, this interface serves to position the sandwich domain in such a way as to close off the gap between strands β2–β3, thereby ensuring the fidelity of the active site. Second, the mouse NMPRTase possesses an additional sequence at the C terminus that corresponds to domain C in yNAPRTase. This segment, which is not present in QAPRTases, is predicted to occupy the same position in both proteins—extending out from above the barrel core (Figure 5A); whether this domain imparts a similar ATP-dependent energetic coupling in NMPRTases or an alternative function is still unclear. In humans, two alternatively spliced isoforms of the NMPRTase gene are distinguished by the presence or absence of this domain C-like element. These are conceptually represented in Figure 5B. Isoform a is 491 amino acids in

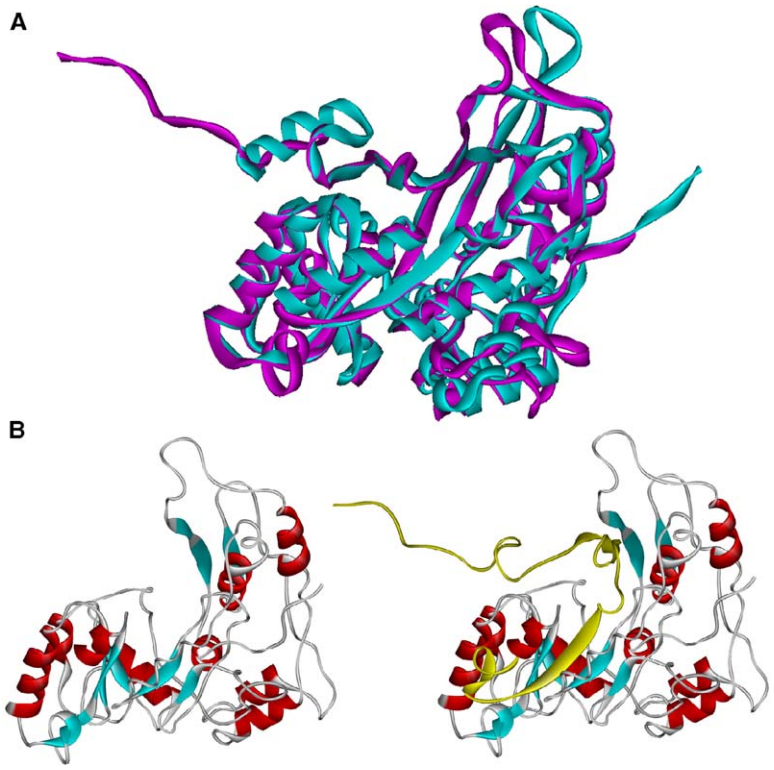

Figure 5. Homology Modeling of NMPRTase

(A) Homology model of the mouse NMPRTase (magenta) generated with the program Modeller and threaded onto the yNAPRTase structure (cyan).

(B) Homology models for the two human NMPRTase isoforms, also generated with Modeller. The structure on the left represents the truncated splice variant lacking the domain C equivalent. The structure on the right depicts the full-length version of the enzyme with the additional sequence at the C terminus similar to yNAPRTase (highlighted in yellow).

length, with 95% identity to the mouse enzyme, while isoform b is 364 residues long and lacks the final C-terminal region. In spite of this truncation, several identical matches to each protein variant exist in the Genbank EST database (dbEST), indicating that each is expressed. The absence of domain C further indicates that the NMPRTase may function efficiently without the requirement of energetic coupling.

Molecular Evolution of Type II PRTases

NAPRTases are monomeric Type II PRTases with important structural similarities to QAPRTases, which suggests a common lineage. Multiple sequence alignments show that NAPRTases and NMPRTases have more insertions than QAPRTases. It is commonly thought that proteins become longer and more complex than their ancestral progenitors as they evolve (Li, 1997; Wang et al., 2005), providing opportunities for functional improvement (Matsuura et al., 1999; Trifonov and Berezovsky, 2003). Insertion distribution implies that NMPRTases are more "modern" than NAPRTases, which in turn are more "modern" than QAPRTases. Fold recognition methods applied to the α/β barrel domain indicate that thiamine phosphate synthase (TMP-PPase; PDB: 1G69) is the closest structural homolog. The use of a pyrophosphate substrate and a catalytic mechanism involving the formation of a carbocation intermediate are additional points of similarity between PRTases and TMP-PPase (Peapus et al., 2001). Rooted phylogenetic trees with TMP-PPase as an outgroup suggest again that QAPRTases are the most divergent family, followed by NAPRTases and NMPRTases (Figure S3). The $\alpha + \beta$ sandwich domain is similar to several single domain transferases. Trees built with the sandwich domain of PRTases show the same topology as those built with the barrel domain. Taxonomic distribution and the acquisition of progressively longer versions of domain C also support a latter divergence of NMPRTases with respect to NAPRTases.

Based on these lines of evidence, we propose a model for the molecular evolution of Type II PRTases (Figure 6). The fact that the sandwich domain is split into two parts in PRTases suggests that an ancestral open enzyme might have arisen from the insertion of an α/β barrel domain into a two-layer sandwich transferase (Figure 6, red arrow), and subsequently stabilized through domain-swapping dimerization. From this ancestral form, the development of new Type II PRTases is likely driven by gene duplication. This is suggested by the presence of paralogous NAPRTases, NMPRTases, and QAPRTases in humans and other organisms. Gene duplication allows existing genes to evolve new functions and fine tune biological processes. In Type II PRTases, such actions afforded the acquisition of two new complementary salvage enzymatic activities, thus considerably improving NAD homeostasis. The addition of a regulatory element (domain C) communicates a tight energetic coupling to NAPRTase catalysis and presumably a different set of restraints on NMPRTase activities. This final constituent shows high variability and possibly plays a number of regulatory roles on the enzymatic activity of NAPRTase and NMPRTase, as illustrated by the presence of multiple NAPRTase and NMPRTase isoforms in humans that

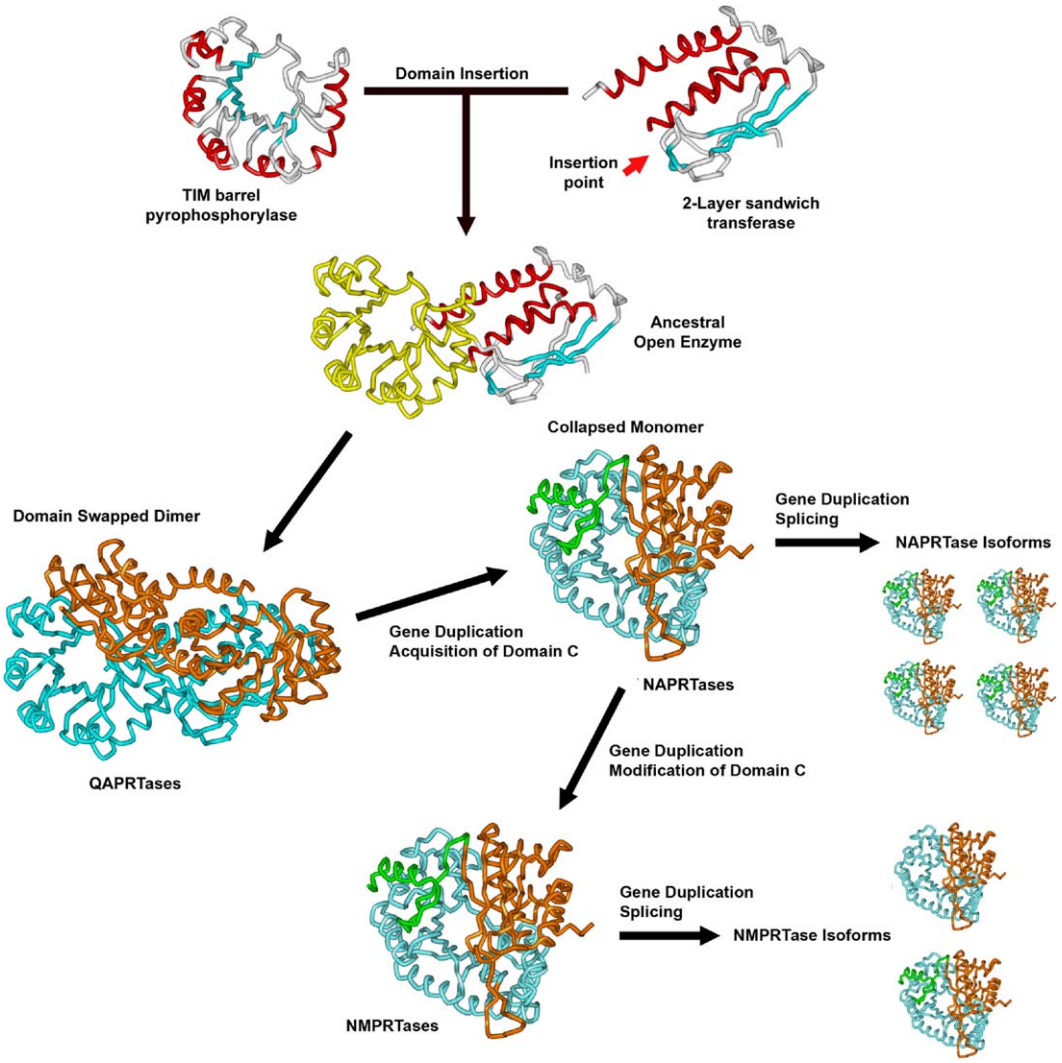

Figure 6. Proposed Model for the Molecular Evolution of Type II PRTases

differ mainly in the length and absence/presence of domain C.

Experimental Procedures

Cloning, Expression, and Purification

yNAPRTase was amplified by PCR from genomic DNA from *S. cerevisiae* by using *PfuTurbo* (Stratagene) and primer pairs encoding the predicted 5′ and 3′ ends of yNAPRTase. The PCR product was cloned into plasmid pMH1, which encodes an expression and purification tag (MGSDKIHHHHHH) at the amino terminus of the full-length protein. The cloning junctions were confirmed by sequencing. Protein expression was performed in a selenomethionine-containing medium by using the *E. coli* methionine auxotrophic strain DL41. Bacteria were lysed by sonication in lysis buffer (50 mM K_2HPO_4 [pH 7.8], 300 mM NaCl, 10% glycerol, 5 mM imidazole, Roche EDTA-free protease inhibitor tablets) with 0.5 mg/ml lysozyme. Immediately after sonication, the cell debris was pelleted by ultracentrifugation at 60,000 × g for 20 min (4°C). The soluble fraction was applied to a gravity flow metal chelate column (Talon resin charged with cobalt; Clontech) equilibrated in lysis buffer. The column was then washed with 7 column volumes (CV) of wash buffer (20 mM Tris [pH 7.8], 300mM NaCl, 10% glycerol, 10 mM imidazole) and eluted with 3 CV of elute buffer (25 mM Tris [pH 7.8], 300 mM NaCl, 150 mM imidazole). The protein was then buffer exchanged into crystallization buffer (10 mM Tris [pH 7.8], 150 mM NaCl) and concentrated by centrifugal ultrafiltration (Orbital). The protein was either frozen in liquid nitrogen for later use or was used immediately for crystallization trials.

Crystallization

The protein was crystallized by using the nanodroplet vapor diffusion method (Santarsiero et al., 2002) with standard JCSG crystallization protocols (Lesley et al., 2002). Crystals were grown at 4°C by using 6%–16% PEG 5000 MME, 0.06 M MES, and 0.04 M NaMES at pH 6 with a protein concentration of 10–30 mg/ml 15–20% ethylene glycol was used as a cryoprotectant for freezing. The crystals were indexed in the triclinic space group P_1 (Table 1).

Data Collection

MAD diffraction data sets, in addition to a 1.75 Å high-resolution data set (λ_0 = 0.9686), were collected at wavelengths corresponding to the inflection point (λ_1 = 0.9798) and the low-energy remote (λ_2 = 1.0332) (Table 1). The data sets were collected at 100 K by

using ADSC 210 and 315 CCD detectors at beamlines 8.2.1 and 8.2.2, respectively, of the Advanced Light Source (ALS, Berkeley, CA, USA). Data were integrated and reduced by using HKL2000 (Otwinowski and Minor, 1997). Data statistics are summarized in Table 1.

Structure Solution and Refinement

The heavy-atom sites were found by using SHELXD (Schneider and Sheldrick, 2002) and were refined with autoSHARP (de La Fortelle and Bricogne, 1997; C. Vonrhein et al., personal communication) by using the inflection and remote wavelength data from 50 Å to 3.0 Å. The peak wavelength of the MAD data suffers from radiation damage and was not used in the phasing. The experimental phases were improved, and an initial trace was obtained by using RESOLVE (Terwilliger and Berendzen, 1999). The trace was further improved with wARP (Perrakis et al., 1997) from the RESOLVE model by using the 1.75 Å data set. Structure refinement (including TLS refinement) was carried out at 1.75 Å by using REFMAC5 (CCP4, 1994; Winn et al., 2001), O (Jones et al., 1991), and Xfit (McRee, 1999). Refinement statistics are summarized in Table 1. The final model includes four protein monomers (residues –1–415 for molecule A, residues 1–419 for molecule B, residues –1–416 for molecule C, and residues 0–415 for molecule D), four bound phosphate molecules, three ethylene glycol molecules, one molecule of morpholineethanesulfonic acid (MES), three chloride ions, and 1272 water molecules in the asymmetric unit. No electron density was observed for residues 416–429 in molecule A, residues 420–429 in molecule B, residues 417–429 in molecule C, residues 416–429 in molecule D, or for the rest of the expression and purification tags besides those residues already denoted (residues –1 and 0).

Structure Analysis

Analysis of the stereochemical quality of the model was accomplished by using the AutoDepInputTool (http://deposit.pdb.org/adit/), MolProbity (Lovell et al., 2003), SFcheck 4.0 (Vaguine et al., 1999), and WHAT IF 5.0 (Vriend, 1990). Protein quaternary structure analysis used the PQS server (http://pqs.ebi.ac.uk/; Henrick and Thornton, 1998).

Biocomputational Methods

Sets of NAPRTases, QAPRTases, and NMPRTases were generated through similarity searches performed with PSI-BLAST (Altschul et al., 1997). The sequences of *S. cerevisiae* NAPRTase (SwissProt: P39683), *Thermotoga maritima* QAPRTase (SwissProt: Q9X1X8), and mouse NMPRTase (GenBank: GI:50293167) were used as queries. Two PSI-BLAST iterations were performed against the NCBI nonredundant database. BLOSUM62 was the weight matrix, the expectation value threshold for inclusion of sequences into a profile was 0.01, and no low-complexity filtering was used. Sequence-based multiple sequence alignments were produced by using the ClustalX implementation of ClustalW 1.8 (Higgins et al., 1994) and the program T-Coffee (Notredame et al., 2000). Multiple sequence alignments integrating sequence and structural data were generated by using the program 3D-Coffee (O'Sullivan et al., 2004). The alignments were visualized, manually curated, and evaluated for residue conservation with the Genedoc sequence alignment editor (Nicholas et al., 1997). Phylogenetic trees were produced by using the Neighbor-Joining method as implemented in ClustalX. Positions with gaps in the multiple sequence alignments were ignored during tree construction. Confidence values for the groupings in the trees were obtained by applying 1000 cycles of bootstrapping. PDB structures were visualized, and molecular graphics, including both ribbon representations and surface graphics, were composed with Discovery Studio ViewerPro 5.0 (Accelrys). Rigid and flexible pairwise structural alignments were created by using the programs CE (Shindyalov and Bourne, 1998) and FATCAT (Ye and Godzik, 2003). Multiple structures were aligned simultaneously by using the program MASS (Dror et al., 2003). The profile-profile method FFAS03 (Rychlewski et al., 2000) was used for fold recognition, to search for distant homologs, and sequence alignment when sequence-sequence or sequence-profile methods did not yield statistically significant results. The structural homology model of mouse NMPRTase was built by using the program Modeller (Fiser and Sali, 2003); the FFAS03 alignment of the mouse NMPRTase and yNAPRTase as alignment input, and the structure of the yNAPRTase was used as a structural template. The information shown in Figure 1 was derived from KEGG (Kanehisa et al., 2004) metabolic maps combined with enzymatic information from the BRENDA enzyme database (Schomburg et al., 2004). The potential ATP binding site in the yNAPRTase was predicted by using SiteEngine (Shulman-Peleg et al., 2004). EST searches were performed by using TBLASTN against the GenBank dbEST database and its human and mouse sections (Boguski et al., 1993).

Supplemental Data

Supplemental Data including a steroview and a wire diagram of the secondary structure of yNAPRTase, active site occupancies and conservation, the template-target sequence alignment used to build the homology model of NMPRTase, and phylogenetic analysis used to propose the molecular evolution model of the Type II PRTase family are available at http://www.structure.org/cgi/content/full/13/9/1385/DC1.

Acknowledgments

The authors thank members of the Joint Center for Structural Genomics that have provided intellectual and material support throughout this project. We also acknowledge Rebecca Page and Vandana Sridhar for suggestions on crystallization and Joseph Arndt for assistance during refinement. We thank Andrei Osterman for invaluable insights and helpful discussions, Anna Cànaves for her assistance in graphics design, and Angela Walker for her support in manuscript preparation. Also, we would like to thank the reviewers for their valuable comments, feedback, and suggestions. These studies were supported by a National Institutes of Health Protein Structure Initiative grant to the Joint Center for Structural Genomics (GM62411).

Received: March 24, 2005
Revised: May 18, 2005
Accepted: May 18, 2005
Published: September 13, 2005

References

Altschul, S.F., Madden, T.L., Schäffer, A.A., Zhang, J., Zhang, Z., Miller, W., and Lipman, D.J. (1997). Gapped BLAST and PSI-BLAST: a new generation of protein database search programs. Nucleic Acids Res. *25*, 3389–3402.

Araki, T., Sasaki, Y., and Milbrandt, J. (2004). Increased nuclear NAD biosynthesis and SIRT1 activation prevent axonal degeneration. Science *305*, 1010–1013.

Bieganowski, P., and Brenner, C. (2004). Discoveries of nicotinamide riboside as a nutrient and conserved NRK genes to establish a Preiss-Handler independent route to NAD^+ in fungi and humans. Cell *117*, 495–502.

Boguski, M.S., Lowe, T.M., and Tolstoshev, C.M. (1993). dbEST–database for "expressed sequence tags." Nat. Genet. *4*, 332–333

Buck, S.W., Gallo, C.M., and Smith, J.S. (2004). Diversity in the Sir2 family of protein deacetylases. J. Leukoc. Biol. *75*, 939–950.

Cao, H., Pietrak, B.L., and Grubmeyer, C. (2002). Quinolinate phosphoribosyltransferase: kinetic mechanism for a type II PRTase. Biochemistry *41*, 3520–3528.

CCP4 (Collaborative Computational Project, Number 4) (1994). The CCP4 suite: programs for protein crystallography. Acta Crystallogr. D *50*, 760–763.

Cho, Y., Sharma, V., and Sacchettini, J.C. (2003). Crystal structure of ATP phosphoribosyltransferase from *Mycobacterium tuberculosis*. J. Biol. Chem. *278*, 8333–8339.

de La Fortelle, E., and Bricogne, G. (1997). Maximum-likelihood heavy atom parameter refinement for the multiple isomorphous replacement and multiwavelength anomalous diffraction methods. Methods Enzymol. *276*, 472–494.

Dror, O., Benyamini, H., Nussinov, R., and Wolfson, H. (2003).

MASS: multiple structural alignment by secondary structures. Bioinformatics *19*, 95–104.

Eads, J.C., Scapin, G., Xu, Y., Grubmeyer, C., and Sacchettini, J.C. (1994). The crystal structure of human hypoxanthine-guanine phosphoribolsyltransferase with bound GMP. Cell *78*, 325–331.

Eads, J.C., Ozturk, D., Wexler, T.B., Grubmeyer, C., and Sacchettini, J.C. (1997). A new function for a common fold: the crystal structure of quinolinic acid phosphoribosyltransferase. Structure *5*, 47–58.

Fiser, A., and Sali, A. (2003). Modeller: generation of refinement of homology-based protein structure models. Methods Enzymol. *374*, 461–491.

Gross, J.W., Rajavel, M., Segura, E., and Grubmeyer, C. (1996). Energy coupling in *Salmonella typhimurium* nicotinic acid phosphoribosyltransferase: identification of His-219 as site of phosphorylation. Biochemistry *35*, 3917–3924.

Gross, J.W., Rajavel, M., and Grubmeyer, C. (1998). Kinetic mechanism of nicotinic acid phosphoribosyltransferase: implications for energy coupling. Biochemistry *37*, 4189–4199.

Grubmeyer, C.T., Gross, J.W., and Rajavel, M. (1999). Energy coupling through molecular discrimination: nicotinate phosphoribosyltransferase. Methods Enzymol. *308*, 28–48.

Henrick, K., and Thornton, J.M. (1998). PQS: a protein quaternary structure file server. Trends Biochem. Sci. *23*, 358–361.

Higgins, D., Thompson, J., Gibson, T., Thompson, J.D., Higgins, D.G., and Gibson, T.J. (1994). CLUSTAL W: improving the sensitivity of progressive multiple sequence alignment through sequence weighting, position-specific gap penalties and weight matrix choice. Nucleic Acids Res. *22*, 4673–4680.

Hughes, K.T., Dessen, A., Gray, J.P., and Grubmeyer, C. (1993). The *Salmonella typhimurium* nadC gene: sequence determination by use of Mud-P22 and purification of quinolinate phosphoribosyltransferase. J. Bacteriol. *175*, 479–486.

Jensen, H.K., Mikkelsen, N., and Neuhard, J. (1997). Recombinant uracil phosphoribosyltransferase from the thermophile *Bacillus caldolyticus*: expression, purification, and partial characterization. Protein Expr. Purif. *10*, 356–364.

Jones, T.A., Zou, J.Y., Cowan, S.W., and Kjeldgaard, M. (1991). Improved methods for building protein models in electron density maps and the location of errors in these models. Acta Crystallogr. *D47*, 110–119.

Kanehisa, M., Goto, S., Kawashima, S., Okuno, Y., and Hattori, M. (2004). The KEGG resource for deciphering the genome. Nucleic Acids Res. *32*, D277–D280.

Katoh, A., and Hashimoto, T. (2004). Molecular biology of pyridine nucleotide and nicotine biosynthesis. Front. Biosci. *9*, 1577–1586.

Kim, C., Xuong, N.H., Edwards, S., Yee, M.C., Spraggon, G., and Mills, S.E. (2002). The crystal structure of anthranilate phosphoribosyltransferase from the enterobacterium *Pectobacterium carotovorum*. FEBS Lett. *523*, 239–246.

Lesley, S.A., Kuhn, P., Godzik, A., Deacon, A.M., Mathews, I., Kreusch, A., Spraggon, G., Klock, H.E., McMullan, D., Shin, T., et al. (2002). Structural genomics of the *Thermotoga maritima* proteome implemented in a high-throughput structure determination pipeline. Proc. Natl. Acad. Sci. USA *99*, 11664–11669.

Li, W.H. (1997). Molecular Evolution (Sunderland, MA: Sinauer Associates).

Lovell, S.C., Davis, I.W., Arendall, B., de Bakker, P.I.W., Word, M.J., Prisant, M.G., Richardson, J.S., and Richardson, D.C. (2003). Structure validation by C-alpha geometry: phi, psi, and C-beta deviation. Proteins *50*, 437–450.

Marcus, S.L., and Balbinder, E. (1972). Purification of anthranilate 5-phosphoribosylpyrophosphate phosphoribosyltransferase from *Salmonella typhimurium* using affinity chromatography: resolution of monomeric and dimeric forms. Biochem. Biophys. Res. Commun. *47*, 438–444.

Matsuura, T., Miyai, K., Trakulnaleamsai, S., Yomo, T., Shima, Y., Mike, S., Yamamoto, K., and Urabe, I. (1999). Evolutionary molecular engineering by random elongation mutagenesis. Nat. Biotechnol. *17*, 58–61.

Matthews, B.W. (1968). Solvent content of protein crystals. J. Mol. Biol. *33*, 491–497.

Mayans, O., Ivens, A., Nissen, L.J., Kirschner, K., and Wilmanns, M. (2002). Structural analysis of two enzymes catalysing reverse metabolic reactions implies common ancestry. EMBO J. *21*, 3245–3254.

McRee, D.E. (1999). XtalView/Xfit - a versatile program for manipulating atomic coordinates and electron density. J. Struct. Biol. *125*, 156–165.

Muiras, M.L. (2003). Mammalian longevity under the protection of PARP-1's multi-facets. Ageing Res. Rev. *2*, 129–148.

Nicholas, K.B., Nicholas, H.B., Jr., and Deerfield, D.W., II. (1997). GeneDoc: analysis and visualization of genetic variation. EMBNEW.NEWS *4*, 14.

Notredame, C., Higgins, D., and Heringa, J. (2000). T-Coffee: a novel method for multiple sequence alignments. J. Mol. Biol. *302*, 205–217.

O'Sullivan, O., Suhre, K., Abergel, C., Higgins, D.G., and Notredame, C. (2004). 3DCoffee: combining protein sequences and structures within multiple sequence alignments. J. Mol. Biol. *340*, 385–395.

Otwinowski, Z., and Minor, W. (1997). Processing of x-ray diffraction data collected in oscillation mode. Methods Enzymol. *276*, 307–326.

Pappas, D.L., Jr., Frisch, R., and Weinreich, M. (2004). The NAD(+)-dependent Sir2p histone deacetylase is a negative regulator of chromosomal DNA replication. Genes Dev. *18*, 769–781.

Peapus, D.H., Chiu, H.-J., Campobasso, N., Reddick, J.J., Begley, T.P., and Ealick, S.E. (2001). Structural characterization of the enzyme-substrate, enzyme-intermediate, and enzyme-product complexes of thiamin phosphate synthase. Biochemistry *40*, 10103–10114.

Perrakis, A., Sixma, T.K., Wilson, K.S., and Lamzin, V.S. (1997). wARP: improvement and extension of crystallographic phases by weighted averaging of multiple refined dummy atomic models. Acta Crystallogr. *D53*, 448–455.

Preiss, J., and Handler, P. (1958a). Biosynthesis of diphosphopyridine nucleotide. I. Identification of intermediates. J. Biol. Chem. *233*, 488–492.

Preiss, J., and Handler, P. (1958b). Biosynthesis of diphosphopyridine nucleotide. II. Enzymatic aspects. J. Biol. Chem. *233*, 493–500.

Rajavel, M., Gross, J., Segura, E., Moore, W.T., and Grubmeyer, C. (1996). Limited proteolysis of *Salmonella typhimurium* nicotinic acid phosphoribosyltransferase reveals ATP-linked conformational change. Biochemistry *35*, 3909–3916.

Rajavel, M., Lalo, D., Gross, J.W., and Grubmeyer, C. (1998). Conversion of a cosubstrate to an inhibitor: phosphorylation mutants of nicotinic acid phosphoribosyltransferase. Biochemistry *37*, 4181–4188.

Revollo, J.R., Grimm, A.A., and Imai, S.I. (2004). The NAD biosynthesis pathway mediated by nicotinamide phosphoribosyltransferase regulates Sir2 activity in mammalian cells. J. Biol. Chem. *279*, 50754–50763.

Rizzi, M., and Schindelin, H. (2002). Structural biology of enzymes involved in NAD and molybdenum cofactor biosynthesis. Curr. Opin. Struct. Biol. *12*, 709–720.

Rongvaux, A., Shea, R.J., Mulks, M.H., Gigot, D., Urbain, J., Leo, O., and Andris, F. (2002). Pre-B-cell colony-enhancing factor, whose expression is up-regulated in activated lymphocytes, is a nicotinamide phosphoribosyltransferase, a cytosolic enzyme involved in NAD biosynthesis. Eur. J. Immunol. *32*, 3225–3234.

Rychlewski, L., Jaroszewski, L., Li, W., and Godzik, A. (2000). Comparison of sequence profiles. Strategies for structural predictions using sequence information. Protein Sci. *9*, 232–241.

Santarsiero, B.D., Yegian, D.T., Lee, C.C., Spraggon, G., Gu, J., Scheibe, D., Uber, D.C., Cornell, E.W., Nordmeyer, R.A., Kolbe, W.F., et al. (2002). An approach to rapid protein crystallization using nanodroplets. J. Appl. Crystallogr. *35*, 278–281.

Schlunegger, M.P., Bennett, M.J., and Eisenberg, D. (1997). Oligo-

mer formation by 3D domain swapping: a model for protein assembly and misassembly. Adv. Protein Chem. *50*, 61–122.

Schneider, T.R., and Sheldrick, G.M. (2002). Substructure solution with SHELXD. Acta Crystallogr. *D58*, 1772–1779.

Schomburg, I., Chang, A., Ebeling, C., Gremse, M., Heldt, C., Huhn, G., and Schomburg, D. (2004). BRENDA, the enzyme database: updates and major new developments. Nucleic Acids Res. *32*, D431–D433.

Schwarzenbacher, R., Jaroszewski, L., von Delft, F., Abdubek, P., Ambing, E., Biorac, T., Brinen, L.S., Canaves, J.M., Cambell, J., Chiu, H.J., et al. (2004). Crystal structure of a type II quinolic acid phosphoribosyltransferase (TM1645) from *Thermotoga maritima* at 2.50 Å resolution. Proteins *55*, 768–771.

Sharma, V., Grubmeyer, C., and Sacchettini, J.C. (1998). Crystal structure of quinolinic acid phosphoribosyltransferase from *Mycobacterium tuberculosis*: a potential TB drug target. Structure *6*, 1587–1599.

Shin, D.H., Oganesyan, N., Jancarik, J., Yokota, H., Kim, R., and Kim, S.H. (2005). Crystal structure of a nicotinate phosphoribosyltransferase from *Thermoplasma acidophilum*. J. Biol. Chem. *280*, 18326–18335.

Shindyalov, I.N., and Bourne, P.E. (1998). Protein structure alignment by incremental combinatorial extension (CE) of the optimal path. Protein Eng. *11*, 739–747.

Shulman-Peleg, A., Nussinov, R., and Wolfson, H.J. (2004). Recognition of functional sites in protein structures. J. Mol. Biol. *339*, 607–633.

Terwilliger, T.C., and Berendzen, J. (1999). Automated structure solution for MIR and MAD. Acta Crystallogr. *D55*, 849–861.

Tickle, I.J., Laskowski, R.A., and Moss, D.S. (1998). Error estimates of protein structure coordinates and deviations from standard geometry by full-matrix refinement of γB- and βB2-crystallin. Acta Crystallogr. *D54*, 243–252.

Trifonov, E.N., and Berezovsky, L.N. (2003). Evolutionary aspects of protein structure and folding. Curr. Opin. Struct. Biol. *13*, 110–114.

Vaguine, A.A., Richelle, J., and Wodak, S.J. (1999). SFCHECK: a unified set of procedures for evaluating the quality of macromolecular structure-factor data and their agreement with the atomic model. Acta Crystallogr. *D55*, 243–252.

Vriend, G. (1990). WHAT IF: a molecular modeling and drug design program. J. Mol. Graph. *8*, 52–56.

Vos, S., de Jersey, J., and Martin, J.L. (1997). Crystal structure of *Escherichia coli* xanthine phosphoribosyltransferase. Biochemistry *36*, 4125–4134.

Wang, D., Hsieh, M., and Li, W.-H. (2005). A general tendency for conservation of protein length across eukaryotic kingdoms. Mol. Biol. Evol. *22*, 142–147.

Winn, M.D., Isupov, M.N., and Murshudov, G.N. (2001). Use of TLS parameters to model anisotropic displacements in macromolecular refinement. Acta Crystallogr. *D57*, 122–133.

Ye, Y., and Godzik, A. (2003). Flexible structure alignment by chaining aligned fragment pairs allowing twists. Bioinformatics *19*, 246–255.

Accession Numbers

Atomic coordinates and experimental structure factors of yNAPRTase have been deposited with the PDB and are accessible under the code 1VLP.